ELSEVIER

Polymer 40 (1999) 5773–5779

polymer

Modulated differential scanning calorimetry: 12. Interphase boundaries and fractal scattering in interpenetrating polymer networks

M. Song, D.J. Hourston*, F.-U. Schafer

IPTME, Loughborough University, Loughborough LE11 3TU, UK

Received 2 April 1998; received in revised form 29 July 1998; accepted 8 September 1998

Abstract

The morphology of polyurethane (PU)–poly(methyl methacrylate) (PEMA) interpenetrating polymer networks (IPNs) were investigated by means of small-angle X-ray scattering (SAXS) and modulated-temperature differential scanning calorimetry (M-TDSC) techniques. Based on the analysis method employed by Tan et al. [Polymer 1997;38:4571], the interfacial thickness in the IPNs was calculated from SAXS data. The conclusion is that the interfacial thickness is zero and there are sharp domain boundaries in the PU-PEMA IPNs. M-TDSC results show that the PU-PEMA IPNs have a multi-phase morphology with a diffuse interphase region. The M-TDSC results are in agreement with DMTA and TEM findings. The M-TDSC, TEM and DMTA results, therefore, conflict with those obtained from the analysis of the SAXS data. We believe that the analysis method employed by Tan et al. is questionable for IPNs. © 1999 Elsevier Science Ltd. All rights reserved.

Keywords: Interpenetrating polymer networks; Fractal; Interfacial thickness

1. Introduction

Small-angle X-ray scattering (SAXS) is a useful technique in the investigation of morphology of the multiphase polymer materials, such as semi-crystalline polymers, polymer blends and block copolymers, especially for the measurements of interfacial thickness [1–3]. Recently, SAXS has been used to study the interphases and fractal behaviour of interpenetrating polymer networks (IPNs) which were prepared by the simultaneous method [4]. The results obtained by Tan et al. [4] showed that the interfacial thickness in certain polyacrylate/ epoxy IPNs was zero and the interface was found to be fractal.

A fractal object is defined as one that shows self-similarity over a range of length scales and where a very simple power-law relationship exists between the magnitude of a measurable property and the size of yardstick used to measure that property [5]. SAXS has been employed in several investigations [6–8] of porous materials such as silicas, coals and aerogels, to determine particle and pore size distribution and to give information about the fractal structure in these materials. For the study of fractal behaviour in the above materials, one important characteristic is that the boundary between phases must be sharp, i.e. there is no interfacial thickness.

From our long experience of IPNs, it is difficult for us to accept that the interfacial thickness in IPNs is zero. It is necessary, however, to know whether or not the analysis method employed by Tan et al. [4] is applicable to the calculation of interfacial thickness in IPNs. In this paper, the interfacial thickness and fractal behaviour in polyurethane (PU)– poly(ethyl methacrylate) (PEMA) IPNs are investigated using the analysis method employed by Tan et al. [4] based on SAXS data, and the analysis results are discussed with relation to the data measured by modulated-temperature differential scanning calorimetry (M-TDSC [9]).

2. Experimental

2.1. Materials

Polyoxypropylene glycol of molar mass 1025 (PPG1025, BDH) was used as the polyurethane (PU) soft segment. The hard segment was formed from 1,1,3,3-tetramethylxylene diisocyanate (TMXDI, CyTec) and the crosslinker was trimethylol propane (TMP, Aldrich). Stannous octoate (SnOC, Sigma) was used as the PU catalyst. Polyethyl methacrylate (PEMA) was formed by crosslinking ethyl methacrylate (EMA, Aldrich) with tetraethylenglycol

* Corresponding author.

PII: S0032-3861(98)00683-1

dimethacrylate(TEGDM, Fluka). Azoisobutyronitrile (AIBN, Fluka) was used as the initiator.

The TMP was dissolved in the PPG1025 at 60°C. At room temperature, the initiator, AIBN, was dissolved in the monomer, EMA, and the crosslinker. Upon addition of the SnOC and the TMXDI, the components were stirred under a nitrogen blanket for 5 min. After degassing for 1 min at high vacuum, the mixture was moulded in an O-ring mould. Curing was conducted in 3 cycles of 24 h at 60, 80 and 90°C.

2.2. SAXS measurements

The SAXS measurements were performed with a Kratky Compact camera (Paar KG) equipped with a one-dimensional position-sensitive detector (Braun). Ni-filtered CuKα radiation ($\lambda = 0.154$ nm) was used. The sample was kept in the camera under vacuum to minimise air scattering. All data were taken at room temperature. They were corrected for absorption, background scattering, slit length smearing and thermal fluctuation. Primary beam intensities were determined in absolute units [e.u.^{2}/nm^3] by using a moving slit method. (The authors gratefully thank Professor I. Alig at Deutsches Kunststoff Institute, Germany for help with the SAXS measurements.)

2.3. M-TDSC

Thermal analysis was subsequently performed using a model 2910 M-TDSC from TA Instruments. Both temperature and baseline were calibrated as for conventional DSC. A scan rate of 3°C/min was used with a temperature modulation period of 60 s and a temperature modulation amplitude of 1.0°C. In order to maximise the signal as well as to reduce the heat transfer delay, an average sample mass of 8–12 mg was used. Nitrogen, at a flow rate of 35 ml/min, was used as the heat transfer gas.

3. Results and Discussion

3.1. Determination of the interfacial thickness in the PU-PEMA IPNs

In this section, we follow Tan's research schedule [4] in that the interphase of the PU-PEMA IPNs was viewed as a smooth surface with thickness σ. σ for IPNs was determined under the context of the theory proposed by Ruland [10].

Small angle X-ray scattering by ideal, two-phase systems with sharp boundaries has been treated by Porod [11]. The scattered intensity at a large value of s ($s = 2/\lambda \sin\theta$, θ is the scattering angle and λ is the wave length of the X-rays) was found to be proportional to the reciprocal fourth power of s.

$$\lim_{s\to\infty} [I(s)] = \mathrm{K}/s^4 \tag{1}$$

K is the Porod law constant. This means that in the large angle region, the product of $I(s)s^4$ becomes constant. However, in polymers, a deviation from the Porod law was observed. Ruland [10] has shown that the Porod law may be modified to include two kinds of deviation, positive deviations and negative deviations. The presence of thermal density fluctuations or mixing within phases results in an enhancement of scattering at high angles. The deviations appear to be due to disorder, thermal motion, or the onset of wide-angle scattering [12,13]. Thermal density fluctuations result in positive deviations from Porod's law. After allowing for this effect, the scattering intensity is given by Eq. 2.

$$\lim_{s\to\infty} [I_{\mathrm{obs}}(s)] = I(s)H^2(s) + I_{\mathrm{b}}(s) \tag{2}$$

$I(s)$ is the Porod law intensity and $H^2(s)$ is the Fourier transform of the autocorrelation of the smoothing function, which causes the negative deviations from Porod's law due to the diffuse interphase. $I_{\mathrm{b}}(s)$ is the scattering background due to electron-density fluctuations within the phases. According to Ruland [10], the scattered intensity at relatively high angles can be fitted empirically by the following relation.

$$I_{\mathrm{b}}(s) = I_{\mathrm{o}}\exp(\mathrm{b}s^2) \tag{3}$$

b is a constant and I_{o} is the intensity value extrapolated to zero angle. If the intensities are absolute, the value of I_{o} (corrected for slit smearing) reflects the magnitude of the thermal density fluctuations. In all scattered intensity data shown in this paper, the observed intensity has been corrected for the background by subtracting the thermal density fluctuation contribution.

The diffuse phase boundary, on the other hand, causes a depletion of high angle scattering resulting in a negative deviation. The electron-density profile, $\Delta\rho_{\mathrm{obs}}(r)$, may be represented as follows.

$$\Delta\rho_{\mathrm{obs}}(r) = \Delta\rho(r)h(r) \tag{4}$$

r is the distance along an arbitrary vector inside the scattering volume. h(r) is a smoothing function, $\Delta\rho(r)$ is the electron-density difference between the two phases.The scattered intensity at a large value of s can be written as

$$\lim_{s\to\infty} [I_{\mathrm{obs}}(s)] = I(s)H^2(s) \tag{5}$$

For the sigmodal-gradient model [10], the smoothing function is Gaussian.

$$H(s) = \exp(-2\pi^2\sigma^2 s^2) \tag{6}$$

and the corresponding Porod law relation becomes

$$I_{\mathrm{obs}}(s) = \mathrm{K}/s^4\exp(-4\pi^2\sigma^2 s^2) \tag{7}$$

For the linear-gradient model [14], the smoothing function is a box function.

$$H(s) = \sin(\pi Es)/(\pi Es) \tag{8}$$

The scattered intensity for this model is given by the

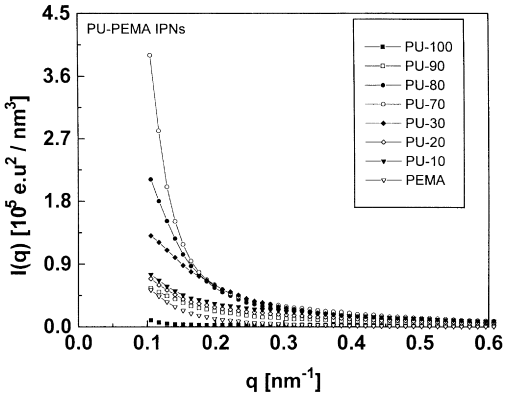

Fig. 1. Scattering intensity $I(q)$ vs. scattering vector q for the PU-PEMA IPNs. (PU-100: PU/PEMA = 100:0; PU-90: PU/PEMA = 90:10; PU-80: PU/PEMA = 80:20; PU-70: PU/PEMA = 70:30; PU-30: PU/PEMA = 30:70; PU-20: PU/PEMA = 20:80; PU-10: PU/PEMA = 10:90 by wt.)

following equation.

$$I_{obs}(s) = K/s^4 \sin^2(\pi Es)/(\pi Es)^2 \quad (9)$$

In Eqs. (7) and (9) σ and E are measures of the diffuseness of the interphase. Comparison of the approximate forms for the intensity of the two models leads to $E = \sqrt{12}\,\sigma$.

Plots of $I(q)$ vs. q ($q = 4\pi/\lambda \sin\theta$) and $\ln[I(s)s^4]$ vs. s^2 for the scattering data from the PU-PEMA IPNs are shown in Figs. 1 and 2, respectively. According to Eq. (5), such plots will give negative slopes for the IPNs with diffuse domain boundaries, and the interphase thickness can be estimated from $[-(\text{slope})/4\pi^2]^{1/2}$. However, for all PU-PEMA IPN samples, the plots had positive slopes. According to these results, the interfacial thickness is zero and there are sharp domain boundaries in the PU-PEMA IPNs.

3.2. Fractal scattering in the PU-PEMA IPNs

The conclusion above is that the interfacial thickness is zero for these PU-PEMA IPNs. In other words, there are sharp domain boundaries. When we view the PU-PEMA IPNs as two-phase systems with sharp, rough boundaries,

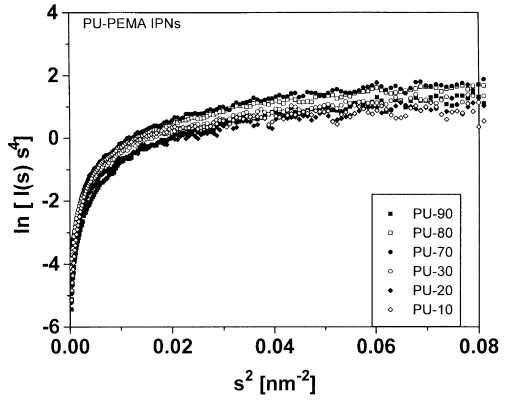

Fig. 2. Plot to evaluate the interfacial thickness parameter s according to Eq. 5 for the PU-PEMA IPNs.

a fractal description may be appropriate. Bale and Schmidt [6] outlined some equations for analysis of X-ray scattering data in the large-q region by considering coal pore surfaces to be fractal. They showed that a fractal surface with dimension $D_s > 2$ obeyed the following correlation function:

$$g(r) = 1 - cr^{3-D_s} \quad (10)$$

where $c = (N_o/4)\,[1/v\phi(1-\phi)]$. v is the sample volume, ϕ is the porosity (volume fraction of the pores), N_o is a constant that depends on the fractal geometry, and D_s is the fractal dimension. Substituting *g(r)* into the general form of the SAXS intensity equation, in the large-q region, gives

$$I(q) \propto q^{D_s-6} \; (D_s < 6) \quad (11)$$

According to this approximation, when the surface is smooth ($D_s = 2$), $I(q)$ is proportional to q^{-4}, in accordance with the Porod law.

There is another kind of fractal: mass fractals [5] that describe a sponge-like structure. For the mass fractal, the correlation function for the interparticle separation has the functional form

$$g(r) \propto r^{D_{m-d}} \; (D_m > d) \quad (12)$$

d is the embedding dimension and D_m is the mass fractal dimension. The scattering intensity is as follows.

$$I(q) \propto q^{-D_m} \quad (13)$$

A system could not behave as a surface fractal and a mass fractal in the same length scale. The length scales in which fractals show self-similarity vary from fractal to fractal. Four critical length scales exist: η, the size of a cluster of pores; ξ, the size of a pore; δ, the size of the smallest rough features on the pore; and a, the atomic spacing. There can be three regions where different power-law equations of $I(q)$ can apply [5,6]:

1. $\eta^{-1} < q < \xi^{-1}$ [the early middle part of the SAXS curves ($0.01\ \text{nm}^{-1} \le s$)], the dimensionality of the pore cluster. If the system is a mass fractal, Eq. (13) is suitable.
2. $\xi^{-1} < q < \delta^{-1}$ [the middle part of the SAXS curves ($s \le 0.1\ \text{nm}^{-1}$)], the dimensionality of the surface. If the surface is a fractal, Eq. (11) holds.
3. $\delta^{-1} < q < a^{-1}$ [the tail of the SAXS curves], the Porod region.

When the PU-PEMA IPNs are viewed as two-phase systems with sharp, rough boundaries (based on the above Results section), the power-law proposed by Porod is no longer valid. Log–log plots of $I(q)$ vs. q are presented in Fig. 3. Straight lines were obtained for the PU-PEMA IPN samples in the larger q range ($0.04 \le s \le 0.22\ \text{nm}^{-1}$). This implies there is surface fractal behaviour [5] in these PU-PEMA systems.

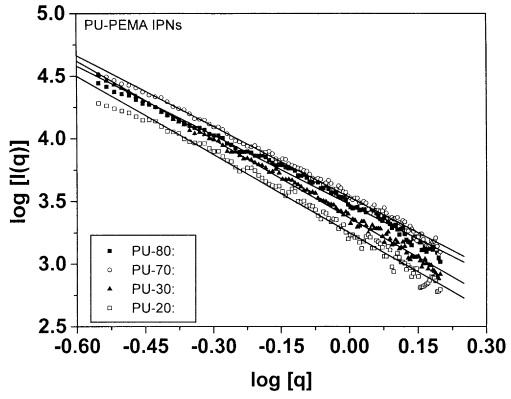

Fig. 3. Log–log plot of $I(q)$ vs. q to show the linear relationship between $I(q)$ and q according to Eqs [9] or [11].

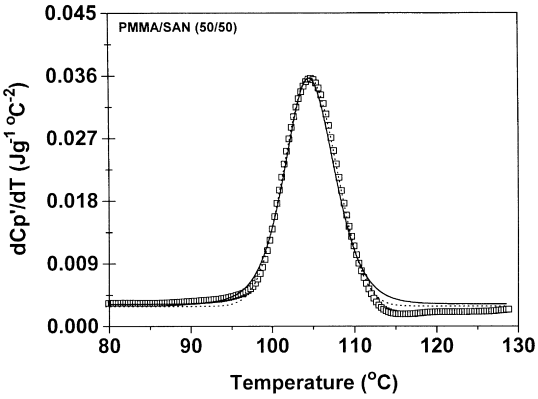

Fig. 5. dC_p'/dT vs. temperature data for experimental (square points), theoretical (solid line) and a Gaussian function (dots) for a miscible blend of poly(methyl methacrylate) and poly(styrene-co-acrylonitrile) (50/50 by wt.).

3.3. M-TDSC results

3.3.1. Theoretical background to M-TDSC analysis in the glass transition region

A differential equation to describe the kinetics of enthalpy (H) relaxation for conventional DSC [15] has been proposed:

$$d\delta/dt = \Delta C_p q - \delta/\tau(T, \delta) \tag{14}$$

In this equation, δ (= H − H_∞) is the excess enthalpy relative to the equilibrium value (H_∞), ΔC_p is the difference between the liquid (C_{p1}) and glassy (C_{pg}) specific heat capacities, q is the heating rate and t is time.

The single relaxation time τ depends upon both T and δ, according to Eq. 15:

$$\tau = \tau_g \exp[-\theta(T - T_g)]\exp[-(1 - x)\theta\delta/\Delta C_p] \tag{15}$$

τ_g is the equilibrium relaxation time at the glass transition temperature T_g, x is the non-linearity parameter ($0 \leq x \leq 1$), and θ is a constant defining the temperature dependence of t. It is given by the following approximation:

$$\theta = \Delta h^*/(RT_g^2) \tag{16}$$

Δh^* is an apparent activation energy. Eqs. (14) and (15) define the response of the glass to any prescribed thermal history.

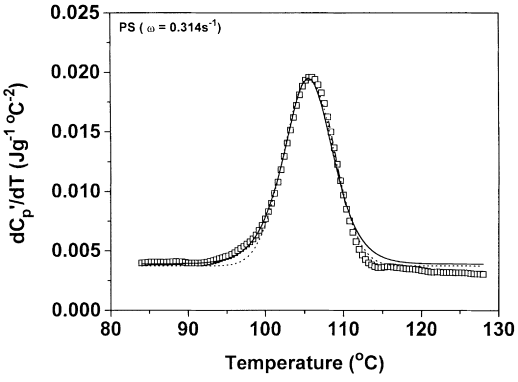

Fig. 4. dC_p'/dT vs. temperature data for experimental (square points), theoretical (solid line) and a Gaussian function (dots) for polystyrene.

The basic principle of M-TDSC is to superimpose upon the conventional DSC heating rate a periodically varying temperature modulation. This modulation is sinusoidal, giving a time dependent temperature [9].

$$T = T_o + qt + A_T \sin(\omega t) \tag{17}$$

T_o is the initial temperature of the DSC scan, A_T is the amplitude of the temperature modulation, and ω is the frequency of modulation.

For M-TDSC [16],

$$dQ/dt = C_{pt}dT/dt + f(t,T) = qC_{pt} + \langle f(t,T)\rangle + \omega A_T C_{p\omega}\cos(\omega t) + C\sin(\omega t) \tag{18}$$

dQ/dt is the heat flow into the sample, C_{pt} is the reversing heat capacity of the sample due to its molecular motions at the heating rate q, $f(t,T)$ is the heat flow arising as a consequence of a kinetically retarded event, $\langle f(t,T)\rangle$ is the average of $f(t,T)$ over the interval of at least one modulation and C is the amplitude of the kinetically retarded response to the temperature modulation. $C_{p\omega}$ is the reversing heat capacity at the frequency ω.

The complex heat capacity is out-of-phase with the heating rate, and a real part, C_p', and an imaginary part, C_p'', may be assigned [14]:

$$C_p' = C_p^* \cos\alpha_i \; C_p'' = C_p^* \sin\alpha_i \; C_p^* = C_p' - iC_p'' \tag{19}$$

where α is the phase angle between heat flow and heating rate.

Assuming $C_p' = A + BT + \phi(T)$ during the glass transition, according to Lacey et al. [17], C_p' can be obtained [18] as follows:

$$C_p' = A + BT + \Delta C_p[1 + \omega^2\tau_g^2\exp(-2\Delta h^*)(RT_g^2)(T - T_g))] \tag{20}$$

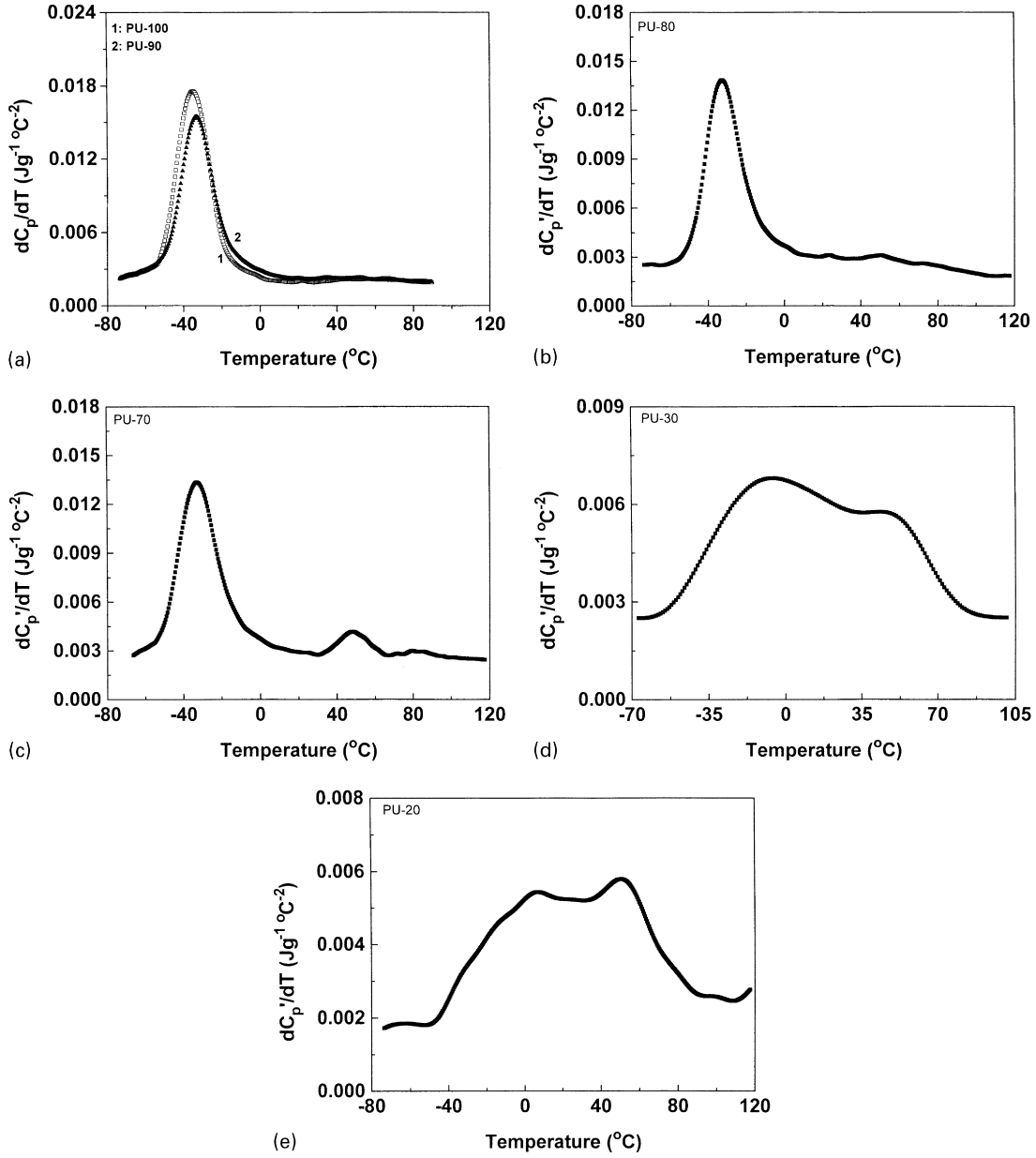

Fig. 6. dC_p'/dT vs. temperature plots for the PU/PEMA IPNs. (a) PU-100 and PU-90; (b) PU-80; (c) PU-70; (d) PU-30 and (e) PU-20.

Figs. 4 and 5 give the comparison of the dC_p'/dT vs. temperature data for experimental (square points), theoretical (solid line) and a Gaussian function (dots) for polystyrene and for a (50/50, by wt.) miscible blend of poly(methyl methacrylate) and poly(styrene-co-acrylonitrile) [19]. Obviously, the experimental data at the glass transition can be described well by the theory, and also by a Gaussian function. For simplicity, in this paper, a Gaussian function is used to describe the change of dC_p'/dT vs. temperature at the glass transition.

3.3.2. Analysis of M-TDSC data

Figs. 6 (a)–(e), show dC_p'/dT vs. temperature for PU100 (PU/PEMA = 100:0), PU-90 (PU/PEMA = 90:10), PU-80, PU-70, PU-30 and PU-20 samples, respectively. Detailed information about the morphology of the PU/PEMA IPNs can be obtained from the dC_p'/dT vs. temperature signals. From these M-TDSC results, it can be concluded that the morphologies of the 80:20, 70:30, 30:70 and 20:80 PU/PEMA IPNs are not two-phase structures containing just the PU-rich and PEMA-rich phases. Their morphologies may be regarded as multiphase in nature with PU-rich and PEMA-rich phases and diffuse boundaries (interfacial phases). Comparing the dC_p'/dT signals of the PU100 and the PU90, it was found that there exists a shoulder on the PU90 transition indicating that the morphology is not a two-phase one.

As shown earlier, for polymers and miscible polymer

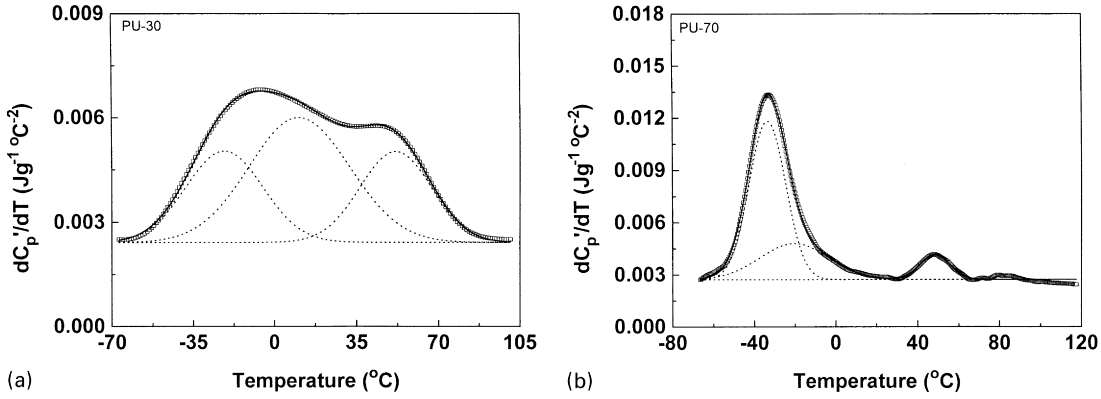

Fig. 7. Experimental data showing peak resolution. (a) PU-30; and (b) PU-70.

blends, the dC_p'/dT vs. temperature signal can be described by a Gaussian function, G, of temperature, the increment of heat capacity, ΔC_p, the glass transition temperature, T_g, and the half width of the glass transition peak (from dC_p'/dT), ω_d.

$$G = \Delta C_p/[\omega d(\pi/2)^{1/2}]\exp[-2(T - T_g)^2/\omega_d^2] \quad (21)$$

For a heterogeneous IPN, it is possible to consider G as a multiple Gaussian function in the transition region.

$$\begin{aligned} G &= \sum Gi(T, T_g i, \omega_{di}, \Delta C_p i) \\ &= \Delta C_{p1}/[\omega_{d1}(\pi/2)^{1/2}]\exp[-2(T - T_{g1})^2/\omega_{d1}^2] \\ &\quad + \Delta C_{p2}/[\omega_{d2}(\pi/2)^{1/2}]\exp[-2(T - T_{g2})^2/\omega_{d2}^2] \\ &\quad + \Delta C_{p3}/[\omega_{d3}(\pi/2)^{1/2}]\exp[-2(T - T_{g1})^2/\omega_{d3}^2] + \ldots. \end{aligned} \quad (22)$$

Gi(T) is related to the *i*-th phase of the multi-phase system. For a multi-phase IPN, the total ΔC_p is the sum of ΔC_{pi} of each phase:

$$\Delta C_p = \sum \Delta C_{pi} \quad (23)$$

By a peak resolution technique, the parameters, ω_{di}, ΔC_{pi} and T_{gi} can be obtained [18].

It may be assumed that interfacial phases exist in these partially compatible PU-PEMA IPNs. The dC_p'/dT signal for the PU-PEMA was divided into three parts by a peak resolution method. These parts are related to PU-rich and PEMA-rich phases and to the interfacial phases. The phase which has the lowest T_g is considered as the PU-rich phase. The phase which has the highest T_g is considered as the PEMA-rich phase. Other phases located between the PU-rich and the PEMA-rich phases are considered as interfacial phases [18].

Figs. 7 (a) and (b) show the peak resolution results for the PU-30 and PU-70 IPNs, respectively. For the PU-30 and PU-70 IPNs, three transition peaks were separated, thus indicating that there are three types of phase structure, PU-rich, PEMA-rich and interfacial phases. Starting from the one-phase mixture of monomers, crosslinkers, initiators and catalysts the polymerisation and crosslinking reactions lead to growing network fragments which then phase separate due to thermodynamic immiscibility.

3.4. On interphase boundaries and fractal scattering in the PU-PEMA IPNs

PU-PEMA is semi-compatible polymer pair [20]. M-TDSC results for the PU-PEMA IPNs are in agreement with that of dynamic mechanical thermal analysis (DMTA) [20]. The micrographs from transmission electron microscopy (TEM) [21] fully confirmed the findings from DMTA [17]. The PEMA (or PU) domains did not exhibit a sharp contrast with PU (or PEMA) matrix [20,21]. The presence of a highly mixed, relatively large interface area was mirrored in the TEM micrographs [22].

The samples studied here are different from those of Tan et al. [4]. The same conclusion has been obtained from the SAXS data analysis. However, our TEM, DMTA and M-TDSC results conflict with those obtained from the SAXS data analysis in that, for all PU-PEMA IPNs samples, the plots resulted in positive slopes, the interphase thickness was zero and there are sharp domain boundaries.

How can this conflict be understood? IPN morphology is clearly multi-phase. Its scattering behaviour may, therefore, be very complex. We believe that the analysis method shown in section 3.1 is questionable. So the analysis method employed by Tan et al. [4] cannot be used to investigate the interphases and fractal behaviour in the PU-PEMA IPNs.

4. Conclusions

M-TDSC results show the morphology of the PU-PEMA IPNs are multi-phase structures. M-TDSC results are in agreement with those of DMTA and TEM. M-TDSC, TEM and DMTA results conflict, however, with those obtained from the SAXS analysis data, for all PU-PEMA IPNs samples. The plots resulted in positive slopes and the interphase thickness was zero, i.e. there are sharp domain boundaries. The analysis method shown in section 3.1 is

questionable for IPNs. The analysis method used by Tan et al. [4] cannot be used to analyse PU-PEMA IPN morphology, to measure the IPN interfacial thickness.

References

[1] Jenkins AD. X-ray scattering of synthetic polymers. New York: Elsevier, 1989.
[2] Perrin P, Prud'homme RE. Macromolecules 1994;27:1852.
[3] Hashimoto T, Todo A, Itoi H, Kawai H. Macromolecules 1977;10:377.
[4] Tan S, Zhang D, Zhou E. Polymer 1997;38:4571.
[5] Mandelbrot BB. The fractal geometry of nature. San Francisco, CA: Freeman, 1983.
[6] Bale HD, Schmidt PW. Phys Rev Lett 1984;53:596.
[7] Avnir D, Farin D, Pfiefer P. Nature 1984;308:261.
[8] Farin D, Volpert A, Avnir DJ. Am Chem Soc 1985;107:3368.
[9] Reading M. Trends in Polym Sci 1993;8:248.
[10] Ruland R. J Appl Crystallogr 1971;4:70.
[11] Porod G. Kolloid Z. 1951;124:94.
[12] Rathje J, Ruland W. Colloid Polym Sci 1976;254:358.
[13] Wiegand W, Ruland W. Prog Colloid Polym Sci 1979;66:355.
[14] Koberstein JT, Morra B, Stein RS. J Appl Cryst 1980;13:34.
[15] Kovacs AJ, Hutchison JM. J Polym Sci: Polym Phys 1976;14:1575.
[16] Reading M, Wilson R, Pollock HM. Proceedings of the 23rd North American Thermal Analysis Society Conference, 1994:2–10.
[17] Jones KJ, Kinshott I, Reading M, Lacey AA, Nikolopoulos C, Pollock HM. Thermochimica Acta 1997;304/305:187.
[18] Song M, Hourston DJ, Schafer F-U, Pollock HM, Hammiche A. Thermochimica Acta 1997;304/305:335.
[19] Song M, Hammiche A, Pollock HM, Hourston DJ, Reading M. Polymer 1995;36:3315.
[20] Hourston DJ, Schafer F-U. High Perform Polym 1996;8:19.
[21] Schafer F-U. PhD thesis, Loughborough University, 1996.
[22] Hourston DJ, Schafer F-U, Bates J, Gradwell MHS. Polymer 1998;39:3311.